Applied Nanoscience (2022) 12:2409–2419
https://doi.org/10.1007/s13204-022-02504-8

ORIGINAL ARTICLE

Facile synthesis of silver and polyacrylic acid doped magnesium oxide nanostructure for photocatalytic dye degradation and bactericidal behavior

Farzana Jamal[1] · Muhammad Ikram[1] · Ali Haider[2] · Anwar Ul-Hamid[3] · Muhammad Ijaz[4] · Walid Nabgan[5,6] · Junaid Haider[7] · Iram Shahzadi[8]

Received: 2 March 2022 / Accepted: 27 April 2022 / Published online: 25 May 2022

Abstract

The presence of cationic dyes in wastewater significantly increase the complexity of processing. Visible-light-trapped inorganic semiconductor for dye degradation has recently become an efficient approach. A convenient one-step co-precipitation process was used to synthesize pristine and doped MgO nanoparticles (NPs). This study aimed to improve the photocatalytic and antibacterial activity of MgO by using different concentrations of Ag (0.03 and 0.06)wt% with a fixed amount of PAA (0.06%). These synthesized samples were used to monitor methylene blue (MB) dye decolourization from an aqueous medium as well as growth inhibition of *Staphylococcus aureus (s.aureus)* and *Escherichia coli (E.coli)*. The structural, morphological and optical properties of MgO and Ag: PAA-MgO were examined using advanced techniques. XRD measurements confirmed hexagonal and cubic phases of MgO and crystallization supresssion upon doping. TEM micrographs revealed hexagonal NPs morphology of MgO. UV–vis spectrophotometer identified a redshift upon doping in absorption spectra and the influence of Ag: PAA on bandgap. A significant improvement in photocatalytic and antibacterial performances was observed for doped NPs with an optimum degradation efficiency (93%) and efficient antibacterial activity towards *S.aureus* indicated by inhibition zone (mm) achieved for Ag: PAA-MgO.

Keywords Co-precipitation · Photocatalysis · Bactericidal · MgO · PAA · Ag

Introduction

Aquatic ecosystems are necessary for human beings' survival, agricultural irrigation and animal production. The rapid industrialization growth and urbanization potential risks are associated with contaminated water increased tremendously owing to industrial effluents; organic dyes, heavy metals (lead, arsenic, mercury, cadmium), pesticides, fertilizers, halogens etc. Organic dyes have been observed as alarming sources for water contamination, cationic dye

✉ Muhammad Ikram
dr.muhammadikram@gcu.edu.pk

✉ Anwar Ul-Hamid
anwar@kfupm.edu.sa

✉ Walid Nabgan
wnabgan@gmail.com

[1] Solar Cell Applications Research Lab, Department of Physics, Government College, University Lahore, Lahore 54000, Punjab, Pakistan

[2] Faculty of Veterinary and Animal Sciences, Muhammad Nawaz Shareef, University of Agriculture, Multan 66000, Punjab, Pakistan

[3] Core Research Facilities, King Fahd University of Petroleum and Minerals, Dhahran 31261, Saudi Arabia

[4] Department of Veterinary Medicine, University of Veterinary and Animal Sciences, Lahore 54000, Punjab, Pakistan

[5] Departament d'Enginyeria Química, Universitat Rovira I Virgili, Av Països Catalans 26, 43007 Tarragona, Spain

[6] School of Chemical and Energy Engineering, Faculty of Engineering, Universiti Teknologi Malaysia, 81310 Skudai, Johor, Malaysia

[7] Tianjin Institute of Industrial Biotechnology, Chinese Academy of Sciences, Tianjin 300308, China

[8] Punjab University College of Pharmacy, University of the Punjab, Lahore 54000, Pakistan

methylene blue (MB) is commonly used in numerous industries like textile, food processing, paint, paper, pharmaceutical, cosmetic and printing. The presence of MB in freshwater resources seriously deteriorates ecological systems and human health, such as vomiting, nausea, eye burns, cyanosis, jaundice, tissue necrosis and mental confusion etc., through inhalation, impact on food chain and drinking water. Additionally, water-born pathogens like Gram positive *Staphylococcus aureus* (*S. aureus*) and Gram-negative *Escherichia coli* (*E. coli*) cause nosocomial infection in humans. Therefore, worldwide challenge is to ensure clean water in the present scenario thus, the elimination of dyes from an aqueous medium is imperative and essential (Sharma et al. 2015; Zulfikar et al. 2020; Moosavi et al. 2020; Khan et al. 2014; Rafatullah et al. 2010; Moniri Javadhesari et al. 2019).

Even though various physiochemical methodologies, membrane separation, coagulation, adsorption, photooxidation, chemical oxidation and electrochemical processes have been documented to decompose organic pollutants from aqueous systems but some are expensive, high energy-consuming and produce secondary hazardous pollution. Thus, to promote existing technologies non-toxic and inexpensive semiconductor photocatalysis has received tremendous attention to control aqueous contaminants (Ikram et al. 2022a; Cheng et al. 2020). Photocatalysis depends on redox reactions caused by photoinduced electrons (e^-) and holes (h^+) on the surface of the heterogeneous photocatalysts. Under this condition, several reactive oxygen species involving water and oxygen are generated because photocatalysts are used practically with water vapor under aerobic conditions. Reactive oxygen species (ROS) are the species to which oxygen converts with high reactivity like singlet oxygen (O_2), superoxide anion radical ($^{\bullet}O^{2-}$), hydrogen peroxide (H_2O_2) and hydroxyl radical ($^{\bullet}OH$). Later, these radicals cause to remove the organic pollutant (dye degradation) from contaminated water (Nosaka and Nosaka 2017; Taghizadeh et al. 2020).

Over the past few decades, nanoscience has proven to be an affordable, scalable and effective tool to synthesize nanomaterials used as photocatalysts and antibacterial to eliminate environmental pollutants. Numerous metal nanomaterials, including silver, gold, platinum, palladium etc., have been widely used as photocatalysts, resulting in high synthetic cost. Therefore, inexpensive metal oxides, zinc, copper, magnesium, nickel and titanium dioxide etc., have been extensively used for photocatalytic dye degradation due to their physicochemical properties; small size, high surface area, and controlled morphology (Nagaraju et al. 2016; Fatima et al. 2017; Ghazal et al. 2021).

One of the existing metal oxides, non-toxic and environmental friendly MgO gained considerable attention for multidimensional applications, photocatalyst, antibacterial, water decontamination, in solar cells and supercapacitors based on superior surface reactivity, chemical and thermal stability, wide energy band gap, low refractive index and dielectric constant (Chanu et al. 2020; Aziz and Karim 2019; Balakrishnan et al. 2020; Sutradhar et al. 2011). In addition, MgO NPs show excellent bactericidal potential because of their low volatility and high-temperature tolerant properties (Ammulu et al. 2021). Various synthesis routes; hydrothermal, sol–gel, laser vaporization, wet chemicals, microwave irradiations, and sonochemical, have been exploited to synthesize MgO nanostructures (Fouda et al. 2021). The eco-friendly and cost-efficient co-precipitation process permits modification in particle size distribution, morphology, agglomeration and surface area, all of which are influenced by pH, reaction temperature, reagent type and concentration. Furthermore, various shapes like lamellar hexagonal, needle, rod, and tube have been obtained by the co-precipitation method (Calderón et al. 2020). Conversely, photocatalytic efficiency is hindered by a wide-bandgap in the ultraviolet (UV) region, which limits the high recombination of photoinduced charge carriers (e^-–h^+) under visible light. Additionally, weak adsorption property and a strong inclination to agglomeration also cause limitations of photocatalytic activity. Besides this, antibacterial activity is also limited, hindering the extensive application of MgO as abactericide (Zeng et al. 2020; Julkapli and Bagheri 2016; Cai et al. 2017).

To strengthen the properties of metal oxides according to requirements, several methods such as tuning, doping with carbon-based materials, polymers, other metals and nonmetals have been suggested to be a promising approach. Doping can significantly improve photocatalytic activity by reducing recombination probabilities of e^- and h^+ (Chanu et al. 2020; Jorfi et al. 2018; Shaheen et al. 2021). Polymers including polyacrylic acid (PAA), polyvinyl alcohol (PVA), poly (methyl methacrylate), polyvinyl pyrrolidone (PVP), etc., have been widely used as dopants owing to low cost, ease of processing (Biswal et al. 2021; Rouabah et al. 2021; Bdewi et al. 2016). Organic polymers doped with inorganic nanomaterials have attracted significant concern to show enhanced properties. PAA exhibited a strong ability to remove heavy metal ions, organic dyes from wastewater, and possesses improved antibacterial properties due to the presence of carboxyl group (COOH). Moreover, PAA based-nanocomposites (PAA-TiO_2) have been extensively applied in solar cells, wastewater treatment, protective covering and optical devices (Rouabah et al. 2021; Tang et al. 2020; Shaik et al. 2016). Moreover, various elements (gold, copper, nickel, iron, chromium, zirconium, silicon, cobalt) have been preferred as dopants for MgO nanomaterials to adjust their optical, electronic and morphological properties (Taşer et al. 2021). In this study, Ag was doped with MgO NPs to extend pholocatalytic activity and bactericidal potential because Ag has a negative influence on the growth of metal oxides, enhanced ROS generation and interaction among

bacterial cells and nanostructures (Cai et al. 2017; Aydoghmish et al. 2019).

In view of the above, pristine and doped MgO NPs with various concentrations wt% of Ag (0.03 and 0.06) and fixed amount of PAA (0.06%) were synthesized using the co-precipitation process. These synthesized products were used as photocatalysts to decompose MB dye and as bactericides to kill *E. coli* and *S. aureus* using ager diffusion technique.

Experimental part

Materials

Poly (acrylic acid ($C_3H_4O_2$))n, magnesium chloride hexahydrate ($MgCl_2.6H_2O$, 99%), sodium hydroxide (NaOH, 98%) and silver nitrate ($AgNO_3$, 99.8%), obtained from Sigma Aldrich (Germany) were used.

Synthesis of MgO and Ag: PAA-MgO

0.5 M of $MgCl_2.6H_2O$ was used to synthesize MgO NPs via co-precipitation method under vigorous stirring at 80 °C for an hour. Afterwards, the required quantity of NaOH was added dropwise to adjust pH > 10, due to which nanostructures settled in the form of a precipitate. Later, these precipitates were centrifuged several times with deionized (DI) water at 7500 rpm, dried overnight at 150 °C and crushed to get a fine powder. Similarly, to synthesize Ag: PAA-MgO NPs various amount of wt% Ag (0.03 and 0.06%) wt% and PAA (0.06%) were incorporated as illustrated in Fig. 1.

Photocatalytic activity

The photocatalytic performance of pristine and doped MgO NPs was evaluated by MB dye decolorization. Initially, an aqueous solution of MB dye was prepared, and pH was adjusted using $NaOH/H_2SO_4$ solution to study dye degradation over pH 4–12. Subsequently, 10 mg photocatalysts were added in suspension under vigorous stirring in dark to ensure adsorption equilibrium between MB dye and photocatalysts. Later, solutions were exposed to a visible light source Hg lamp (400 W, 20 cm) for up to 120 min, and ~ 3 mL of irradiating suspension was periodically removed every 30 min to determine photocatalytic dye degradation through a UV–visible spectrophotometer. According to Beer–Lambert law, dye concentration is directly proportional to its absorbance monitored in the absorption band (λ_{max} = 665 nm). The optimum MB dye absorbance was determined as a function of time intervals, and degradation (%) was calculated as:

$$\text{Degradation } \% = \left(C_o - C_t\right)/C_o \times 100\%$$

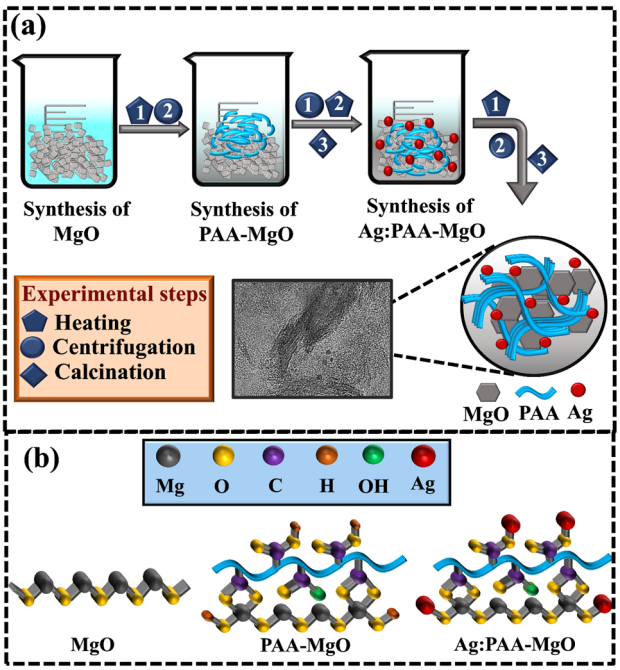

Fig. 1 **a** Schematic illustration of Ag: PAA-MgO NPs synthesis, **b** chemical structure of reactants

where C_o and C_t are MB concentrations before and after light irradiation.

Bactericidal evaluation

Agar based diffusion approach was exploited to evaluate bactericidal behaviour of pristine and doped MgO by inhibition zone measurement contrary to Gram-positive (*S. aureus*) and Gram-negative (*E. coli*) by swabbing 0.5 McFarland on mannitol salt agar and MacConkey (MSA and MA), respectively. Samples of sheep milk (mastitis-positive) were collected from local farms and veterinary clinics in Punjab, Pakistan, refined on 5% blood agar (SBA) and maturated at 37 °C for 24 h. To isolate *S. aureus* and *E. coli,* the cultured isolates were streaked in triplicate on MSA and MA. Under aseptic conditions, sterile cork borer was deployed for 6 mm diameter wells on the MSA and MA plates with different sample concentrations (0.5 and 1.0 mg/0.05 mL) of Ag: PAA-MgO (0:0–1, 0:0.06–1, 0.03:0, 0.06–1, 0.06:0.06–1) filled as minimum and maximum dose into each well correlated to DI water (0.055 mL) and ciprofloxacin (0.005 mg/0.05 mL) as positive and negative controls, correspondingly.

Materials characterization

The crystal structure and phase information of synthesized samples was determined through XRD with Cu Kα radiation (λ = 0.0154 nm and 2θ = 10°–70°). Chemical analysis and

functional groups were undertaken using an FTIR spectrometer (4000–480 cm^{-1}) Surface morphology and Interlayer spacing of prepared nanostructure were inspected through EDX spectrometer and HR-TEM JEOL JEM 2100F. UV–vis spectrophotometer (Genesys 10S) was employed to examine optical properties ranging from 210 to 450 nm.

Results and discussion

The phase purity and crystallinity of pristine and doped MgO NPs were analyzed through XRD in the $2\theta = 10 - 70°$ range (Fig. 2a). Diffraction peaks at 18.7° (001), 38.0° (002), 51.2° (012), 59.0° (110) 62.5° (111) were attributed to a hexagonal phase of MgO NPs (JCPDS no 96–900-2349), and broadness of peaks indicated size reduction (Munusamy et al. 2020). Furthermore, peaks at 32.0° (111), 45.9° and 57.0° (221) corresponded to the cubic phase of MgO NPs (JCPDS no 01–076-1363). The monoclinic $MgCO_3$ diffraction peak was revealed at 27° (-202) evidenced by (JCPDS no 00–020-0669). The addition of PAA resulted in the suppression of crystallization and peaks broadness due to its amorphous nature (Liew et al. 2016; Mantilaka et al. 2014). Furthermore, upon Ag doping, additional diffraction peaks at 29° (211) can be observed (JCPDS no 1–0856), and intensity decreases as the full width at half maximum (FWHM) increases which exhibits influence on crystallinity of MgO NPs. Meanwhile, peaks shifting towards smaller angles demonstrated inter-layer d-spacing increment (Cai et al. 2017). FTIR spectral analysis was performed to access functional groups observed in pristine and doped MgO NPs; corresponding spectra were plotted between 4000 and 500 cm^{-1} as elaborated in Fig. 2(b). Pristine MgO NPs spectrum revealed O–H stretching attributed to its hygroscopic nature, C–O stretching and Mg–O bending and stretching vibrations at 3699, 1450, 867 and 548 cm^{-1}, respectively (Ikram et al. 2021; Tlili et al. 2021; Arshad et al. 2017). Moreover, upon PAA doping, adsorbed water molecules and surface O–H groups manifested their presence by a band with a large half-width at ~3600–3000 cm^{-1} and an additional peak observed at 1395 cm^{-1} assigned to symmetric stretching of COO^- (Hu et al. 2015; Marasini et al. 2021). There was no notable shift

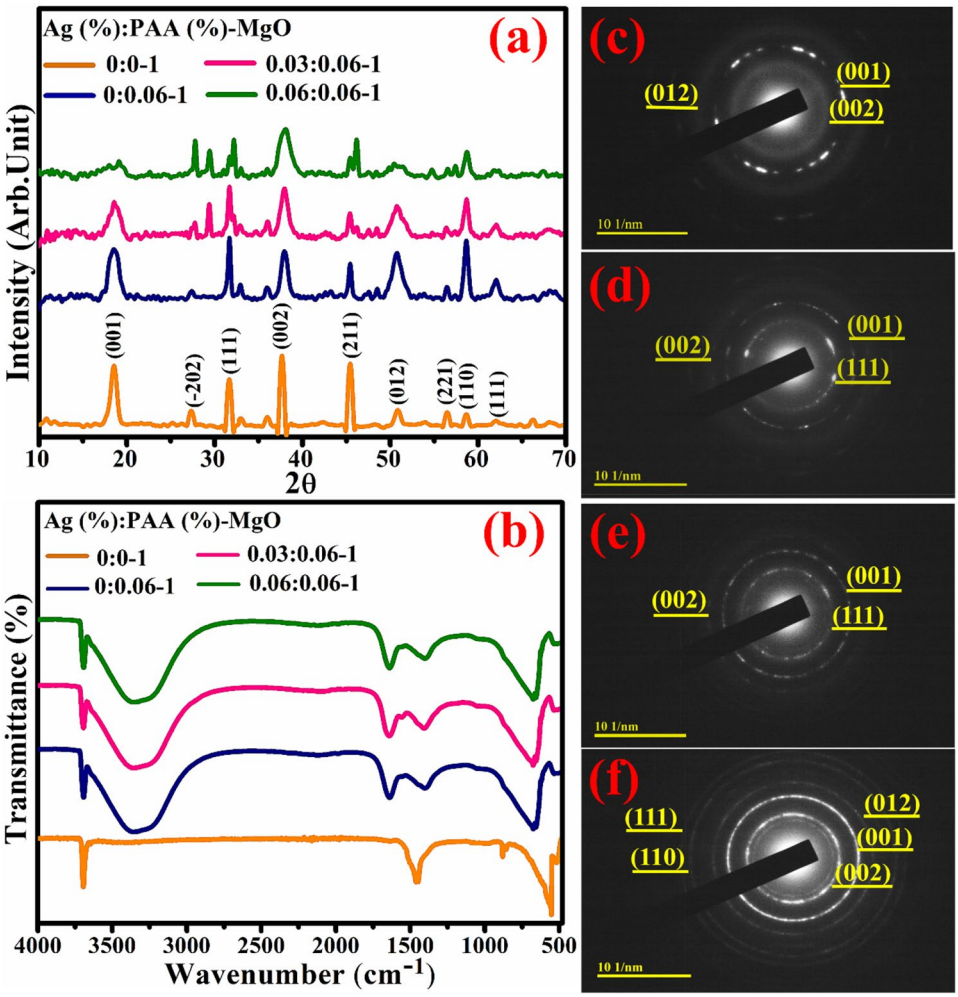

Fig. 2 **a** XRD pattern, **b** FTIR spectra, **c–f** SAED pattern of pristine and doped MgO NPs

in the transmittance spectra with Ag doping. The selected area diffraction (SAED) pattern was recorded by directing electron beams on NPs that revealed distinct diffraction rings, corresponding to the polycrystalline nature of MgO as illustrated in Fig. 2c–f (Das et al. 2018).

The optical characteristics were evaluated using a UV–vis spectrophotometer in the wavelength range 200 – 700 nm. Consequently, MgO absorption bands observed at ~ 313 nm can be endorsed to oxygen vacancies F_2^{2+} center (Pathak et al. 2016). This optical absorption spectra of MgO NPs in the UV region indicated its smaller size (Ulwali et al. 2021). Moreover, absorption peaks of PAA wt% (0.06) and Ag (0.03 and 0.06%) doped MgO NPs were found around 328–341 nm. Results showed that upon doping absorption increases accompanied by redshift, suggesting morphological effects having several active sites or might be quantum confinement effect. Since MgO is a direct bandgap semiconductor, bandgap energy (E_g) values (3.96–3.63 eV) were determined by Tauc's equation, as depicted in Fig. 3.

The morphology of synthesized products was analyzed by TEM analysis as shown in Fig. 4a–d.

The randomly oriented hexagonal structure of the control sample (MgO) is shown in Fig. 4a. The addition of PAA to MgO demonstrated network formation, overlapped to aggregated hexagonal NPs (Fig. 4b). This aggregation is represented by strong and dense collectives NPs, whilst the loosely joined NPs represent the agglomeration that may be broken by mechanical force. As the addition of polymer to NPs causes agglomeration/aggregation, leading to reduce the potential improvement in mechanical properties of NPs owing to the interfacial area restriction (Ashraf et al. 2018). Subsequently, incorporation of Ag into PAA-MgO showed agglomeration of a non-uniformly distributed polymer network with NPs, which increased gradually with an increasing amount of Ag (Fig. 4c, d).

The calculated d-spacing using Gatan software of synthesized product is represented in Fig. 5a–d. The doped free sample (MgO) has inter-layer spacing ~ 0.17 nm (Fig. 5a), well-matched with XRD crystallographic plane (012). PAA doped MgO showed no noticeable change in calculated lattice spacing (Fig. 5b), confirming the overlapping of chain with MgO as stated earlier. The Ag addition to PAA-MgO shows a significant increase in d-spacing from ~ 0.17 to 0.23 nm, indicating proper Ag doping in network-based NPs (Fig. 5c, d).

The atomic arrangement of synthesized NPs was measured with mapping results which explained uniformly dispersed Ag, Cu, Ca, Na, Cl, Mg and O in higher doped specimens (Fig. 6a). To elucidate the elemental composition of synthesized NPs, energy-dispersive X-ray (EDX) spectrometry was employed (Fig. 6b–e). Mg, O and Cl peaks confirmed MgO preparation from $MgCl_2.6H_2O$ precursor. Additionally, Na, Cu and Au peaks were assigned to NaOH solution for adjusting pH, copper grid and coating material to coat non-conductive samples, respectively (Alaizeri et al. 2021).

The photocatalytic MB dye degradation with synthesized photocatalysts were shown 56.92, 65.20, 46.96 and 38.13% in neutral medium (pH = 7), 41.74, 37.21, 36.86 and 31.82% in acidic medium (pH = 4) and 59.69, 92.05, 93.37, 92.91% in basic medium (pH = 12) respectively (Fig. 7). Acquired results depicted synthesized NPs absorb light to generate electron–hole pair that can oxidize or reduce organic dye. The photodegradation rate depends upon electrostatic interaction among dye molecules and catalysts surface (Kong et al. 2010). The pH of the solution is a key factor for photocatalysis that influences the surface charge of dye molecules and catalysts. In an acidic medium, positively charged catalysts surface oppose cationic species adsorption. The surface becomes negatively charged between cationic dye and negatively charged catalyst in the basic medium due to strong electrostatic interaction. As MB is a cationic dye, alkaline pH favours its high degradation by negatively charged surface MgO catalyst while modest degradation in acidic medium (Ikram et al. 2022b; Gh et al. 2015). Later, with PAA doping, degradation efficiency increases based

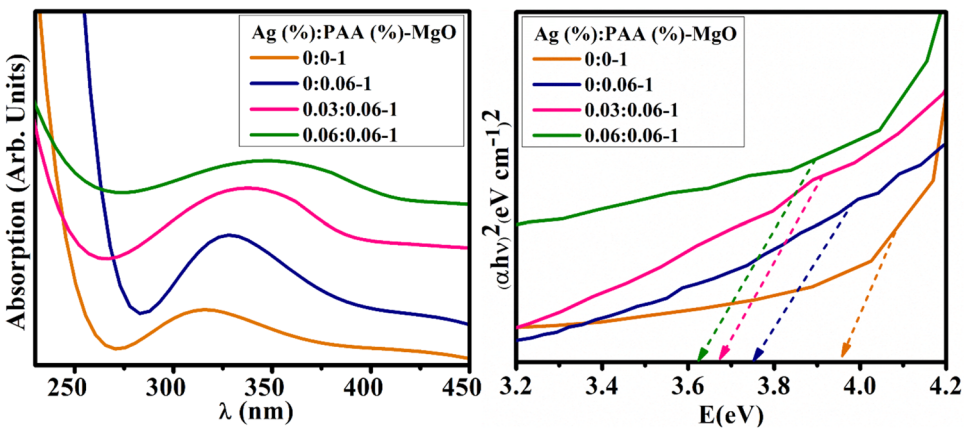

Fig. 3 **a** Absorption spectra, **b** band gap energy plot of pristine and doped MgO

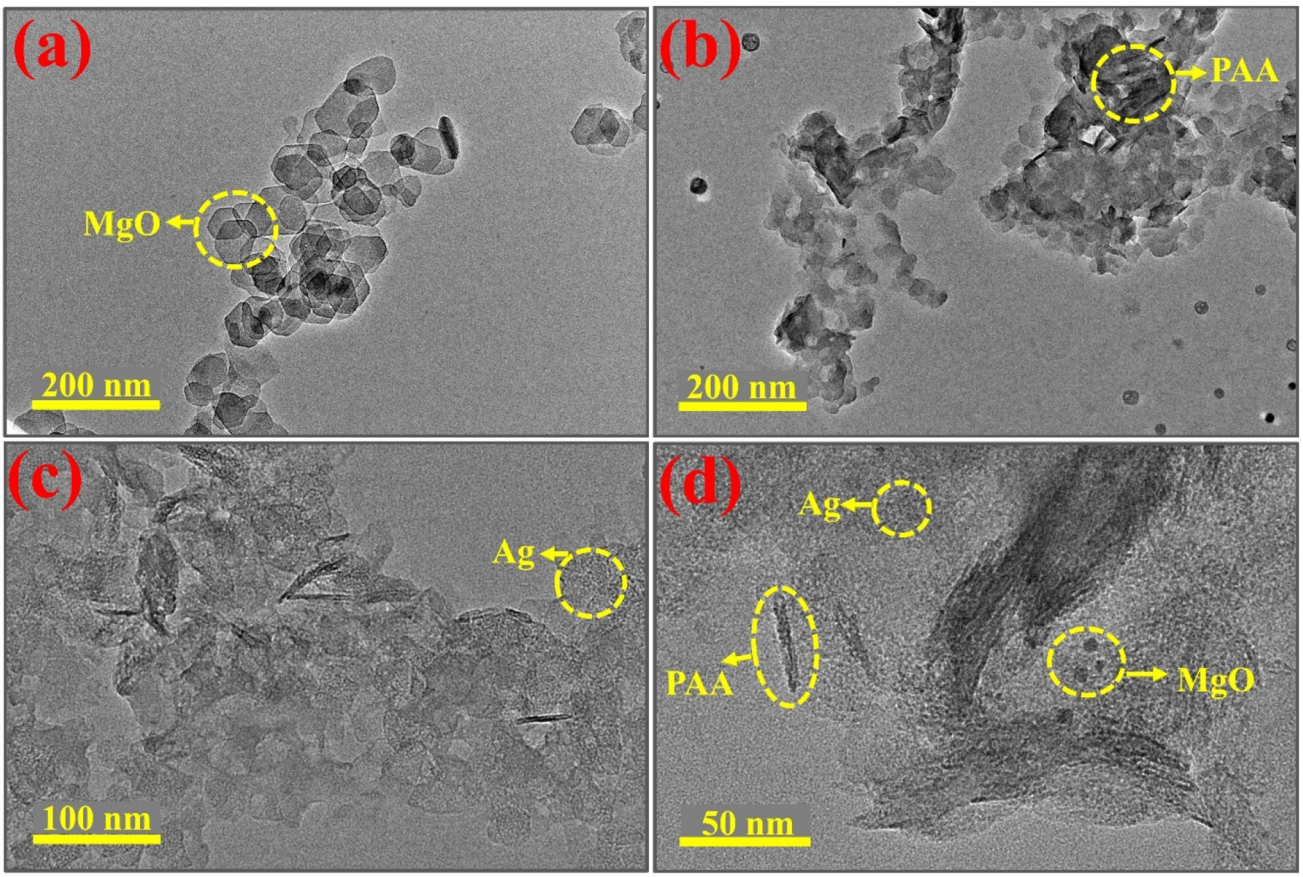

Fig. 4 TEM microstructures of Ag (%): PAA (%)-MgO. **a** 0:0–1, **b** 0:0.06–1, **c** 0.03:0.06–1, **d** 0.06:0.06–1

on carboxyl group (–COOH), which favours ionic, covalent, hydrogen bonding with NPs, ionization of –COOH depends on pH and ionic strength (Liew et al. 2016). Results suggested that the degradation efficiency of Ag: PAA-MgO was higher than pristine MgO NPs, and the highest photocatalytic activity was achieved by 0.03% Ag doping, this was because the degradation efficiency decreased as Ag concentration increased. Furthermore, Ag loading can occupy active sites on the MgO surface, thus, resisting oxygen adsorption (Cai et al. 2017). In addition, dye degradation rate reduces because the high-level concentration of materials causes particle aggregation, which significantly reduces active sites on catalyst surfaces (Alharthi et al. 2020).

The photocatalytic dye degradation in an aqueous solution mainly takes place through photogenerated electron–hole (e^{-}–h^{+}) pair, hydroxyl ($^{\bullet}OH$) and superoxide ($O_2^{\bullet-}$) radicals (Zheng et al. 2019). To determine the photocatalytic activity of MgO NPs and the influence of reactive species on MB dye degradation, the possible photocatalytic dye degradation mechanism was explained below (Shaheen et al. 2021). The photocatalytic activity of MgO NPs begins with photoexcitation of e^{-} from valence band (VB) to conduction band (CB), generating h^{+} in VB. The introduction of Ag and PAA to MgO decreased the Eg, so the photogenerated electrons in MgO can easily transfer towards lower CB of (PAA-MgO), similarly holes will move towards higher potential of PAA-MgO as shown in Fig. 8.

$$MgO + hv \rightarrow MgO\,(e^{-} + h^{+}) \quad (1)$$

The photogenerated e^{-} reacts with dissolved molecular oxygen (O_2) adsorbed on its surface, forming superoxide radical anions ($O_2^{\bullet-}$).

$$e^{-} + O_2 \rightarrow O_2^{\cdot-} \quad (2)$$

Furthermore, these $O_2^{\bullet-}$ radicals react with water (H_2O) molecules and produce oxidizing agents like hydroperoxyl ($H_2O^{\bullet}$) and $OH^{\bullet}$ radicals, acting as reactive agents to degrade organic contaminants.

$$O_2^{\cdot-} + H_2O^{\cdot} \rightarrow HO_2^{\cdot} + OH^{\cdot} \quad (3)$$

Simultaneously, photogenerated h^{+} in VB reacts with H_2O and hydroxide anions (OH^{-}) to form highly active $^{\bullet}OH$ radical.

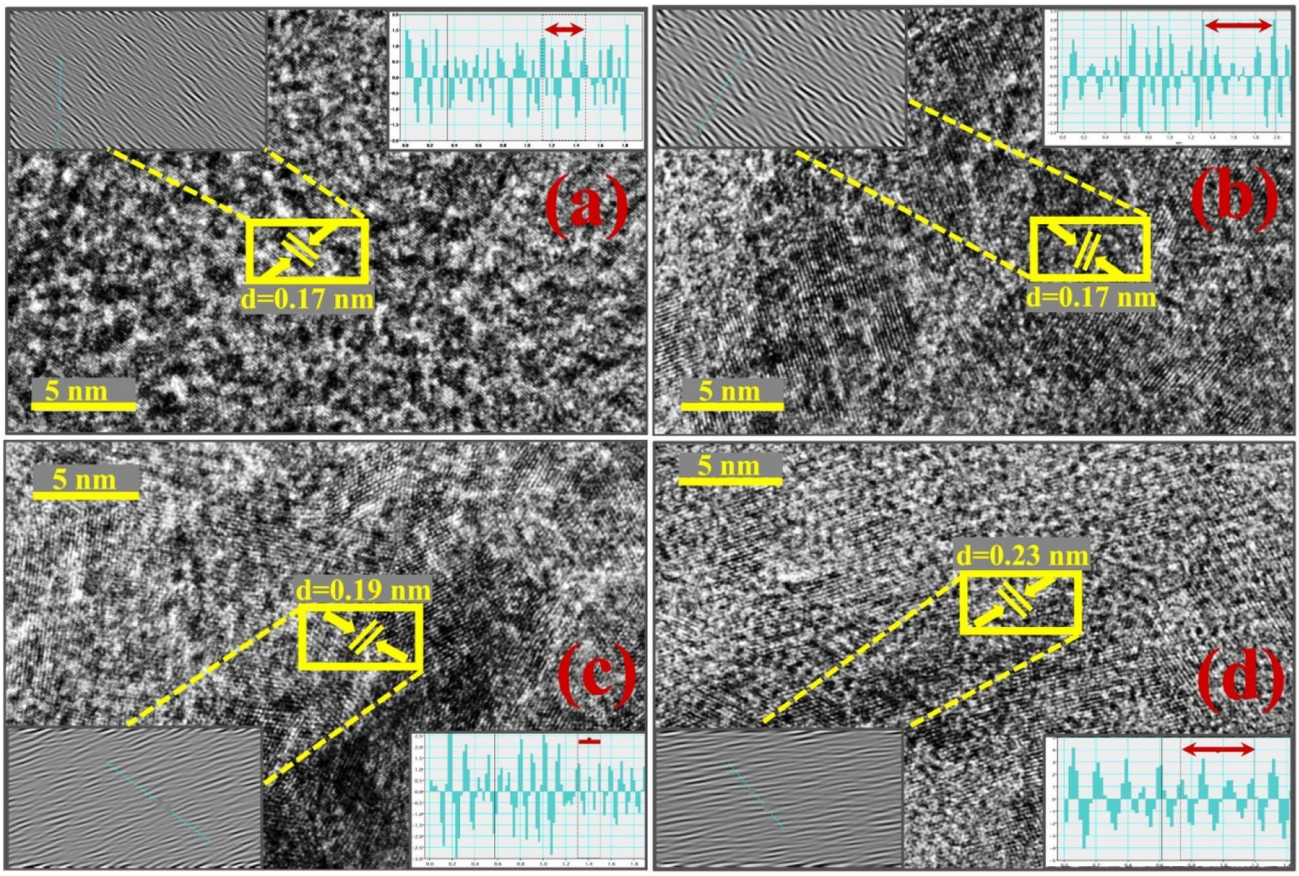

Fig. 5 Inter planar spacing calculated from HR-TEM images of Ag (%): PAA (%)-MgO, **a** 0:0–1, **b** 0:0.06–1, **c** 0.03:0.06–1, **d** 0.06:0.06–1

$$h^+ + H_2O \rightarrow OH^{\cdot} + H^+ \quad (4)$$

$$h^+ + OH^- \rightarrow OH^{\cdot} \quad (5)$$

Hence, $O_2^{\cdot-}$ and $^{\cdot}OH$ radicals strongly oxidize organic contaminants into non-hazardous products (CO_2, H_2O, etc.).

$$(O_2^{\cdot-},\ HO^{\cdot}) + \text{Organic dye (MB)} \rightarrow CO_2 + H_2O \quad (6)$$

The bactericidal potential of pristine and doped MgO NPs was evaluated against *S. aureus and E. coli* using a well diffusion assay, as shown in Table 1. Significant inhibition regions were noticed as (1.55–5.15 mm), (2.10–10.05 mm) for *E. coli* and (0–11.60 mm), (1.30–16.75 mm) for *S. aureus* at a minimum and maximum concentrations, separately. Correspondingly, the results were compared using – ve control DI water (0 mm) and + ve control ciprofloxacin (11.25 mm) inhibition regions for *E. coli and S. aureus*. Results depicted MgO NPs superior bactericidal performance towards *E. coli than S. aureus* because the cell wall of *E. coli* consists of a primarily thin layer of peptidoglycan and outer membrane, but *S. aureus* bacteria consists of a thick layer of peptidoglycan (Tang and Lv 2014). Further, upon PAA doping, carboxylic and hydroxyl groups presence enhanced the ROS generation, facilitating Mg metal ions discharge and, consequently, bacterial cell death (Albalwi et al. 2021). Experimental results showed that PAA dopant improves the antibacterial activity of MgO towards *S. aureus* bacteria (Beyli et al. 2018). Furthermore, Ag doping exhibited more substantial bactericidal effects because Ag has a detrimental influence on metal oxides grain development, resulting in particle size reduction and increased contact among MgO NPs and bacterial cells [19].

The bactericidal activity of MgO NPs against *S.aureus* (Gram-positive) and *E.coli* (Gram-negative) was performed. Gram-positive bacteria contain a dense protective peptidoglycan layer irrespective of the thin layer with the additional outer membrane of Gram-negative bacteria (Slavin et al. 2017), as illustrated in Fig. 9. The bactericidal potential is linked with ROS generation dependent upon factors including surface area, crystallinity, surface oxygen vacancies and diffusion capability (Karthik et al. 2019). The oxygen vacancies on MgO NPs surface adsorb O_2 originated from bacteria reacting with e^- to generate $O2^{\bullet-}$ radical, which further reacts with H_2O to generate H_2O_2, and $^{\bullet}OH$. However, due to excess ROS generation,

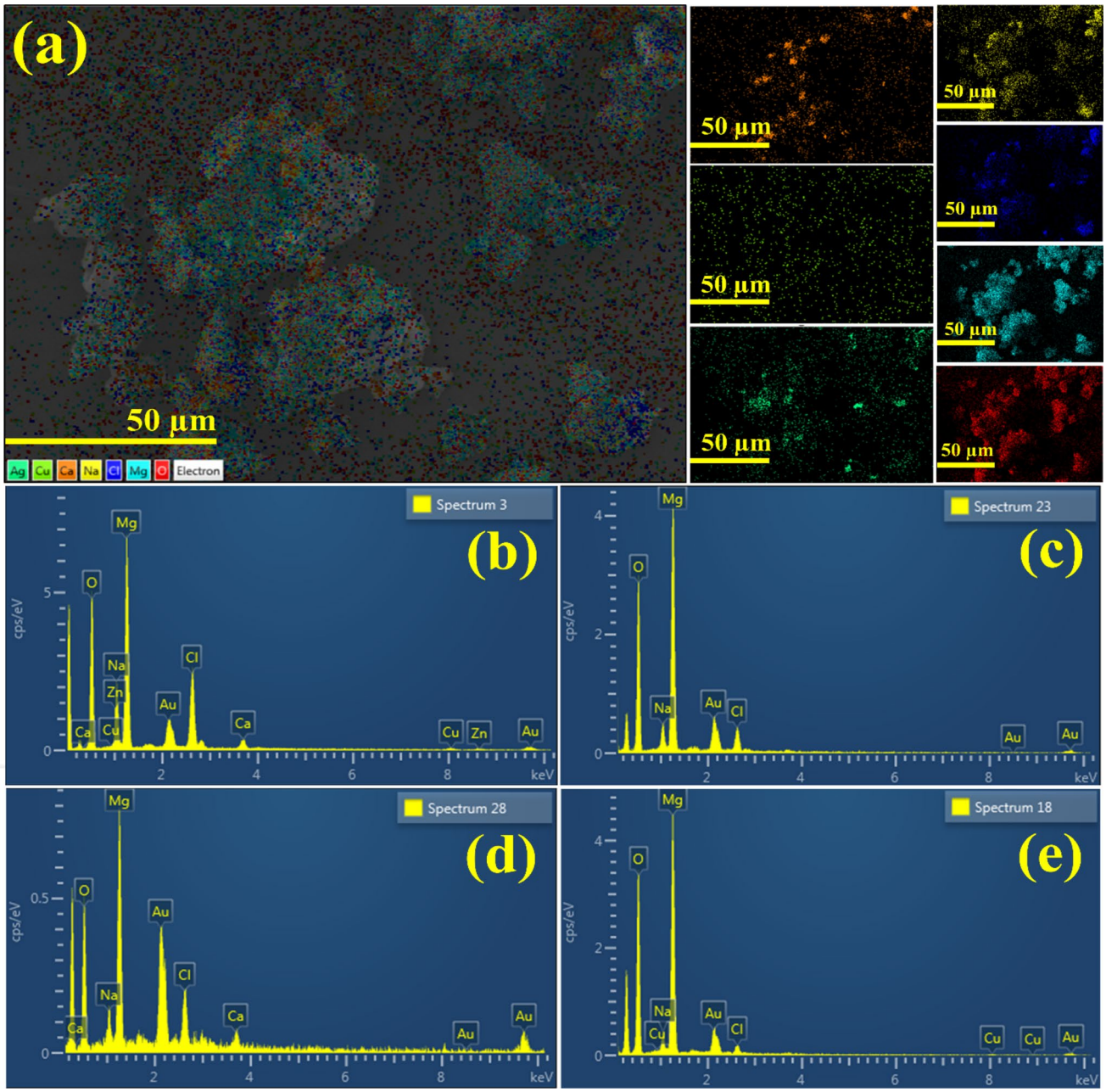

Fig. 6 **a** Mapping of (0.06: 0.06–1) depicted all components distribution, **b**–**e** EDX of 0:0–1, 0:0.06–1, 0.03:0.06–1 and 0.06:0.06–1 respectively

enzymes cannot neutralize it, thus causing oxidative stress on bacterial cells leading to cell necrosis (Bhattacharya et al. 2021). Moreover, the positively charged surface of MgO NPs used as a potential antibacterial agent towards negatively charged bacterial cell membrane by electrostatic action, membrane distortion, cytoplasmic material leakage, DNA degradation, and proteins denaturation (Das et al. 2018; Li et al. 2022) (Fig. 9).

Conclusion

In this study, different Ag concentrations and fixed amounts of PAA-MgO NPs (0:0–1, 0.0.06–1, 0.03:0.06–1 and 0.06:0.06–1) were synthesized via a simple co-precipitation process to determine antibacterial and photocatalytic activity. XRD pattern endorsed hexagonal and

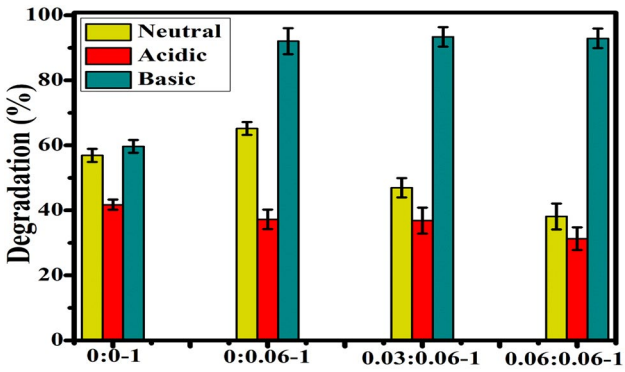

Fig. 7 Photocatalytic dye degradation (%) by Ag (%): PAA (%)-MgO in **a** neutral, **b** acidic and **c** basic medium

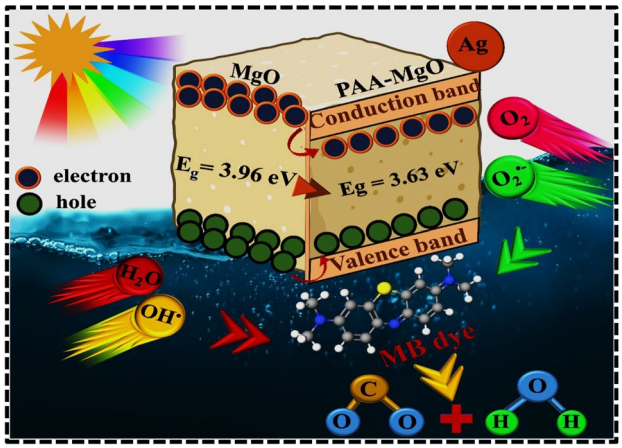

Fig. 8 Schematic illustration of photocatalysis mechanism of pristine and doped MgO NPs

Table 1 Antibacterial activity of Ag: PAA-MgO NPs (0:0–1, 0:0.06–1, 0.03:0.06–1, 0.06:0.06–1)

Samples	*S. aureus* inhibition region (mm)		*E. coli* inhibition region (mm)	
	0.5 mg/50 µL	1.0 mg/ 50 µL	0.5 mg/50 µL	1.0 mg/50 µL
0:0–1	0	1.30	1.55	2.10
0:0.06–1	4.05	6.25	3.75	5.95
0.03:0.06–1	10.55	15.05	4.85	8.90
0.06:0.06–1	11.60	16.75	5.15	10.05
Ciprofloxacin	11.25	11.25	11.25	11.25
DI water	0	0	0	0

cubic structure of MgO, indicating a decrease in crystallinity by the incorporation of dopants. Meanwhile, Mg-O vibrations at 867 and 548 cm^{-1} and polycrystalline nature was affirmed using FTIR and SAED. HR-TEM and EDS

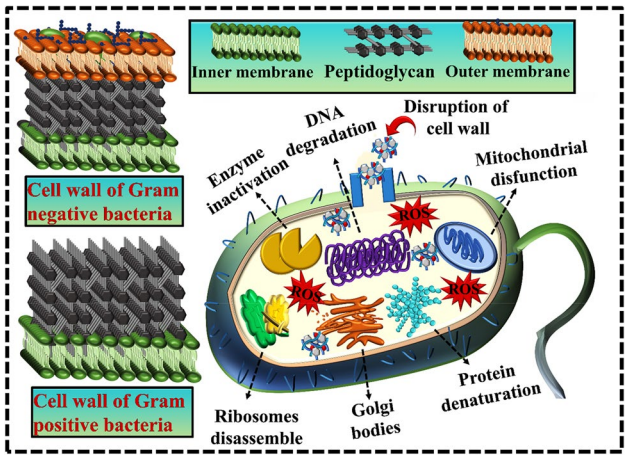

Fig. 9 Schematic antibacterial mechanism expression of MgO NPs

studies confirmed hexagonal nanoparticles morphology of MgO, overlapping of polymer with MgO, and Ag doping increased agglomerations in PAA-MgO. The interplanar spacing increased gradually from 0.17 to 0.23 nm upon Ag doping, and no significant change was observed upon PPA doping, confirming the network overlapped with MgO. The elemental composition confirmed the presence of Mg, O, C and Ag. UV spectra revealed redshift upon doping led to gradual decrease in band gap energy from 3.96 to 3.63 eV. MB dye degradation (%) implies the enhanced visible-light-driven photocatalytic performance in the order Ag: PAA-MgO > PAA-MgO > MgO. The optimum dye degradation rate (93%) was observed for Ag: PAA-MgO. Furthermore, the bactericidal potential of prepared NPs was identified against *S. aureus* and *E. coli* bacteria, while upon doping, superior antibacterial activity towards *S.aureus* was observed gradually.

Acknowledgements The authors are grateful to HEC, Pakistan, for funding through NRPU-20-17615.

Funding This article was funded by Higher Education Commission, Pakistan (20-17615).

Declarations

Conflict of interest This manuscript is free from conflict of interest.

References

Alaizeri ZM, Alhadlaq HA, Aldawood S, Akhtar MJ, Amer MS, Ahamed M (2021) Facile synthesis characterization, photocatalytic activity, and cytotoxicity of Ag-doped MgO nanoparticles. Nanomaterials 11:2915

Albalwi H, Abou El Fadl FI, Ibrahim MM, Abou Taleb MF (2021) Antibacterial impact of acrylic acid/polyvinyl alcohol/MgO

various nanocomposite hydrogels prepared by gamma radiation. Polym Bull 1:1–13

Alharthi FA, Alghamdi AA, Al-Zaqri N, Alanazi HS, Alsyahi AA, Marghany AE, Ahmad N (2020) Facile one-pot green synthesis of Ag–ZnO Nanocomposites using potato peeland their Ag concentration dependent photocatalytic properties. Sci Rep 10:1–14

Ammulu MK, Vinay Viswanath K, Giduturi AK, Vemuri PK, Mangamuri U, Poda S (2021) Phytoassisted synthesis of magnesium oxide nanoparticles from Pterocarpus marsupium roxb heartwood extract and its biomedical applications. J Genet Eng Biotechnol 19:21

Arshad A, Iqbal J, Siddiq M, Mansoor Q, Ismail M, Mehmood F, Ajmal M, Abid Z (2017) Graphene nanoplatelets induced tailoring in photocatalytic activity and antibacterial characteristics of MgO/graphene nanoplatelets nanocomposites. J Appl Phys 121:024901

Ashraf MA, Peng W, Zare Y, Rhee KY (2018) Effects of size and aggregation/agglomeration of nanoparticles on the interfacial/interphase properties and tensile strength of polymer nanocomposites. Nanoscale Res Lett 13:1–7

Aydoghmish SM, Hassanzadeh-Tabrizi S, Saffar-Teluri A (2019) Facile synthesis and investigation of NiO–ZnO–Ag nanocomposites as efficient photocatalysts for degradation of methylene blue dye. Ceram Int 45:14934–14942

Aziz BK, Karim MA (2019) Efficient catalytic photodegradation of methylene blue from medical lab wastewater using MgO nanoparticles synthesized by direct precipitation method. React Kinet Mech Catal 128:1127–1139

Balakrishnan G, Velavan R, Batoo KM, Raslan EH (2020) Microstructure, optical and photocatalytic properties of MgO nanoparticles. Res Phys 16:103013

Bdewi SF, Abdullah OG, Aziz BK, Mutar AA (2016) Synthesis, structural and optical characterization of MgO nanocrystalline embedded in PVA matrix. J Inorg Organometal Polym Mater 26:326–334

Beyli PT, Doğan M, Gündüz Z, Alkan M, Turhan Y (2018) Synthesis, characterization and their antimicrobial activities of boron oxide/poly (acrylic acid) nanocomposites: thermal and antimicrobial properties. Adv Mater Sci 18:28–36

Bhattacharya P, Dey A, Neogi S (2021) An insight into the mechanism of antibacterial activity by magnesium oxide nanoparticles. J Mater Chem B 9:5329–5339

Biswal A, Sethy PK, Swain SK (2021) Change in orientation of polyacrylic acid and chitosan networks by imprintment of gold nanoparticles. Polym Plast Technol Mater 60:182–194

Cai Y, Wu D, Zhu X, Wang W, Tan F, Chen J, Qiao X, Qiu X (2017) Sol-gel preparation of Ag-doped MgO nanoparticles with high efficiency for bacterial inactivation. Ceram Int 43:1066–1072

Calderón DJ, DeAlba-Montero I, Ruiz F, Echeverría F (2020) Effect of synthesis variables on the characteristics of magnesium hydroxide nanoparticles and evaluation of the fluorescence of functionalised Mg (OH) 2 nanoparticles. Adv Nat Sci Nanosci Nanotechnol 11:025008

Chanu LA, Singh KJ, Devi KN (2020) Study on the photocatalytic activity of metal oxide nanoparticles towards the degradation of some organic dyes. Integr Ferroelectr 204:90–99

Cheng J, Zhan C, Wu J, Cui Z, Si J, Wang Q, Peng X, Turng L-S (2020) Highly efficient removal of methylene blue dye from an aqueous solution using cellulose acetate nanofibrous membranes modified by polydopamine. ACS Omega 5:5389–5400

Das B, Moumita S, Ghosh S, Khan MI, Indira D, Jayabalan R, Tripathy SK, Mishra A, Balasubramanian P (2018) Biosynthesis of magnesium oxide (MgO) nanoflakes by using leaf extract of Bauhinia purpurea and evaluation of its antibacterial property against *Staphylococcus aureus*. Mater Sci Eng C 91:436–444

Fatima S, Ali SI, Iqbal MZ, Rizwan S (2017) The high photocatalytic activity and reduced band gap energy of La and Mn co-doped BiFeO 3/graphene nanoplatelet (GNP) nanohybrids. RSC Adv 7:35928–35937

Fouda A, Hassan SE-D, Saied E, Hamza MF (2021) Photocatalytic degradation of real textile and tannery effluent using biosynthesized magnesium oxide nanoparticles (MgO-NPs), heavy metal adsorption, phytotoxicity, and antimicrobial activity. J Environ Chem Eng 9:105346

Gh AB, Sabbaghan M, Mirgani Z (2015) A comparative study on properties of synthesized MgO with different templates. Spectrochim Acta Part A Mol Biomol Spectrosc 137:1286–1291

Ghazal S, Khandannasab N, Hosseini HA, Sabouri Z, Rangrazi A, Darroudi M (2021) Green synthesis of copper-doped nickel oxide nanoparticles using okra plant extract for the evaluation of their cytotoxicity and photocatalytic properties. Ceram Int 47:27165–27176

Hu X, Wei W, Qi X, Yu H, Feng L, Li J, Wang S, Zhang J, Dong W (2015) Preparation and characterization of a novel pH-sensitive Salecan-g-poly (acrylic acid) hydrogel for controlled release of doxorubicin. J Mater Chem B 3:2685–2697

Ikram M, Abid N, Haider A, Ul-Hamid A, Haider J, Shahzadi A, Nabgan W, Goumri-Said S, Butt AR, Kanoun MB (2022b) Towards efficient dye degradation and bactericidal behavior of Mo-doped La2O3 nanostructures. Nanoscale Adv 4:926–942

Ikram M, Imran M, Hayat S, Shahzadi A, Haider A, Naz S, Ul-Hamid A, Nabgan W, Fazal I, Ali S (2022a) MoS 2/cellulose-doped ZnO nanorods for catalytic, antibacterial and molecular docking studies, Nanoscale. Advances 4:211–225

Ikram M, Inayat T, Haider A, Ul-Hamid A, Haider J, Nabgan W, Saeed A, Shahbaz A, Hayat S, Ul-Ain K (2021) Graphene oxide-doped MgO nanostructures for highly efficient dye degradation and bactericidal action. Nanoscale Res Lett 16:1–11

Jorfi S, Pourfadakari S, Kakavandi B (2018) A new approach in sonophotocatalytic degradation of recalcitrant textile wastewater using MgO@ Zeolite nanostructure under UVA irradiation. Chem Eng J 343:95–107

Julkapli NM, Bagheri S (2016) Magnesium oxide as a heterogeneous catalyst support. Rev Inorg Chem 36:1–41

Karthik K, Dhanuskodi S, Gobinath C, Prabukumar S, Sivaramakrishnan S (2019) Fabrication of MgO nanostructures and its efficient photocatalytic, antibacterial and anticancer performance. J Photochem Photobiol B Biol 190:8–20

Khan MDA, Akhtar A, Nabi SA, Khan MA (2014) Synthesis, characterization, and photocatalytic activity of polyaniline-Sn (IV) iodophosphate nanocomposite: its application in wastewater detoxification. Ind Eng Chem Res 53:15253–15260

Kong J-Z, Li A-D, Li X-Y, Zhai H-F, Zhang W-Q, Gong Y-P, Li H, Wu D (2010) Photo-degradation of methylene blue using Ta-doped ZnO nanoparticle. J Solid State Chem 183:1359–1364

Li X, Feng Y, Li H, Zhang Q (2022) Effect of anionic groups on the antibacterial activity of magnesium oxide nanoparticles. Colloids Surf A Physicochem Eng Aspects 635:127978

Liew C-W, Ng H, Numan A, Ramesh S (2016) Poly (acrylic acid)–based hybrid inorganic–organic electrolytes membrane for electrical double layer capacitors application. Polymers 8:179

Mantilaka M, Pitawala H, Karunaratne D, Rajapakse R (2014) Nanocrystalline magnesium oxide from dolomite via poly (acrylate) stabilized magnesium hydroxide colloids. Colloids Surf A Physicochem Eng Aspects 443:201–208

Marasini S, Yue H, Ho SL, Park J, Kim S, Jung K-H, Cha H, Liu S, Tegafaw T, Ahmad MY (2021) Synthesis, Characterizations, and 9.4 tesla T2 MR images of polyacrylic acid-coated terbium (III) and holmium (III) oxide nanoparticles. Nanomaterials 11:1355

Moniri Javadhesari S, Alipour S, Mohammadnejad S, Akbarpour MR (2019) Antibacterial activity of ultra-small copper oxide (II) nanoparticles synthesized by mechanochemical processing against *S. aureus* and *E. coli*. Mater Sci Eng C 105:110011

Moosavi S, Li RYM, Lai CW, Yusof Y, Gan S, Akbarzadeh O, Chowhury ZZ, Yue X-G, Johan MR (2020) Methylene blue dye photocatalytic degradation over synthesised Fe3O4/AC/TiO2 nano-catalyst: degradation and reusability studies. Nanomaterials 10:2360

Munusamy TD, Sarmin S, Ong HR, Gan WT, Hong CS, Khan M, Rahman M (2020) Catalytic performance and antimicrobial activity of Mg (OH) 2/MgO colloidal nanoparticles in alkyd resin nanocomposite derived from palm oil. Polym Bull 77:4571–4586

Nagaraju G, Nagabhushana H, Basavaraj R, Raghu G, Suresh D, Rajanaika H, Sharma S (2016) Green, nonchemical route for the synthesis of ZnO superstructures, evaluation of its applications toward photocatalysis, photoluminescence, and biosensing. Cryst Growth Des 16:6828–6840

Nosaka Y, Nosaka AY (2017) Generation and detection of reactive oxygen species in photocatalysis. Chem Rev 117:11302–11336

Pathak N, Ghosh PS, Gupta SK, Kadam RM, Arya A (2016) Defects induced changes in the electronic structures of MgO and their correlation with the optical properties: a special case of electron–hole recombination from the conduction band. RSC Adv 6:96398–96415

Rafatullah M, Sulaiman O, Hashim R, Ahmad A (2010) Adsorption of methylene blue on low-cost adsorbents: a review. J Hazard Mater 177:70–80

Rouabah N, Boudine B, Nazir R, Zaabat M, Alqahtani AS, Alqahtani MS, Syed R (2021) Nanocomposite synthesis of silver doped magnesium oxide incorporated in PVC matrix for photocatalytic applications. J Polym Res 28:1–10

Shaheen M, Bhatti IA, Ashar A, Mohsin M, Nisar J, Almoneef MM, Iqbal M (2021) Synthesis of Cu-doped MgO and its enhanced photocatalytic activity for the solar-driven degradation of disperse red F3BS with condition optimization. Z Phys Chem 235:1395–1412

Shaik MR, Kuniyil M, Khan M, Ahmad N, Al-Warthan A, Siddiqui MRH, Adil SF (2016) Modified polyacrylic acid-zinc composites: synthesis, characterization and biological activity. Molecules 21:292

Sharma K, Singh G, Kumar M, Bhalla V (2015) Silver nanoparticles: facile synthesis and their catalytic application for the degradation of dyes. RSC Adv 5:25781–25788

Slavin YN, Asnis J, Häfeli UO, Bach H (2017) Metal nanoparticles: understanding the mechanisms behind antibacterial activity. J Nanobiotechnol 15:1–20

Sutradhar N, Sinhamahapatra A, Pahari SK, Pal P, Bajaj HC, Mukhopadhyay I, Panda AB (2011) Controlled synthesis of different morphologies of MgO and their use as solid base catalysts. J Phys Chem C 115:12308–12316

Taghizadeh MT, Siyahi V, Ashassi-Sorkhabi H, Zarrini G (2020) ZnO, AgCl and AgCl/ZnO nanocomposites incorporated chitosan in the form of hydrogel beads for photocatalytic degradation of MB, *E. coli* and *S. aureus*. Int J Biol Macromol 147:1018–1028

Tang Y, Li Y, Zhang Y, Mu C, Zhou J, Zhang W, Shi B (2020) Non-swelling silica–poly (acrylic acid) composite for efficient and simultaneous removal of cationic dye, heavy metal, and surfactant-stabilized emulsion from wastewater. Ind Eng Chem Res 59:3383–3393

Tang Z-X, Lv B-F (2014) MgO nanoparticles as antibacterial agent: preparation and activity. Braz J Chem Eng 31:591–601

Taşer A, Güldüren ME, Güney H (2021) Tuning PL emission energy and bandgap with Ni dopant of MgO thin films. Ceram Int 47:15792–15800

Tlili M, Nefzi C, Alhalaili B, Bouzidi C, Ajili L, Jebari N, Vidu R, Turki Kamoun N (2021) Synthesis and characterization of MgO thin films obtained by spray technique for optoelectronic applications. Nanomaterials 11:3076

Ulwali RA, Abass NK, Majed MD, Alwally HA (2021) Green synthesis of MgO NPs by Olea Europeae leaves extract from Bulk MgO and study physical properties. NeuroQuantology 19:114–119

Zeng W, Yin Z, Gao M, Wang X, Feng J, Ren Y, Wei T, Fan Z (2020) In-situ growth of magnesium peroxide on the edge of magnesium oxide nanosheets: ultrahigh photocatalytic efficiency based on synergistic catalysis. J Colloid Interface Sci 561:257–264

Zheng Y, Cao L, Xing G, Bai Z, Huang J, Zhang Z (2019) Micro-scale flower-like magnesium oxide for highly efficient photocatalytic degradation of organic dyes in aqueous solution. RSC Adv 9:7338–7348

Zulfikar MA, Maulina D, Nasir M, Handayani N, Handajani M (2020) Removal of methylene blue from aqueous solution using poly (acrylic acid)/SiO2 and functionalized poly (acrylic acid)/SiO2 composite nanofibers. Environ Nanotechnol Monit Manag 14:100381